NeuroImage 251 (2022) 119023

Contents lists available at ScienceDirect

NeuroImage

journal homepage: www.elsevier.com/locate/neuroimage

Functional assessment of bidirectional cortical and peripheral neural control on heartbeat dynamics: A brain-heart study on thermal stress

Diego Candia-Rivera [a,*], Vincenzo Catrambone [a], Riccardo Barbieri [b], Gaetano Valenza [a]

[a] Bioengineering and Robotics Research Center E. Piaggio and Department of Information Engineering, School of Engineering, University of Pisa, Pisa 56122, Italy
[b] Department of Electronics, Informatics and Bioengineering, Politecnico di Milano, Milano 20133, Italy

ARTICLE INFO

Keywords:
Brain-heart interplay
Physiological modeling
Synthetic data generation
Sympathovagal estimation
Cold-pressor test
Heart rate variability

ABSTRACT

The study of functional Brain-Heart Interplay (BHI) from non-invasive recordings has gained much interest in recent years. Previous endeavors aimed at understanding how the two dynamical systems exchange information, providing novel holistic biomarkers and important insights on essential cognitive aspects and neural system functioning. However, the interplay between cardiac sympathovagal and cortical oscillations still has much room for further investigation. In this study, we introduce a new computational framework for a functional BHI assessment, namely the Sympatho-Vagal Synthetic Data Generation Model, combining cortical (electroencephalography, EEG) and peripheral (cardiac sympathovagal) neural dynamics. The causal, bidirectional neural control on heartbeat dynamics was quantified on data gathered from 26 human volunteers undergoing a cold-pressor test. Results show that thermal stress induces heart-to-brain functional interplay sustained by EEG oscillations in the delta and gamma bands, primarily originating from sympathetic activity, whereas brain-to-heart interplay originates over central brain regions through sympathovagal control. The proposed methodology provides a viable computational tool for the functional assessment of the causal interplay between cortical and cardiac neural control.

1. Introduction

Recent studies on brain-body interactions showed that neural processing of bodily signals contributes to the subjective perception of the environment, bodily-self, and inner mental states (Azzalini et al., 2019; Blanke and Metzinger, 2009; Candia-Rivera et al., 2021a; Park et al., 2016; Petzschner et al., 2019). In fact, while brain regions responding to autonomic changes are part of interoceptive awareness networks (Craig, 2009, 2002; Khalsa et al., 2009), the neural signaling to the heart continuously interacts with the cerebral structures involved in cardiac processing and nervous-system-wise homeostasis (Critchley and Harrison, 2013); such functional interactions in a wide-sense refer to functional brain-heart interplay (BHI).

Because of its comprehensive definition, the assessment of functional BHI may be linked to the activity of several brain structures that are part of relevant networks, i.e., the central-autonomic network, linked to autonomic control (Silvani et al., 2016; Thayer and Lane, 2009; Valenza et al., 2020, 2019), and the default mode network, which shares components with the aforementioned network (Thayer et al., 2012) and participates in the neural monitoring of cardiac inputs for self-related cognition and conscious perception (Babo-Rebelo et al., 2016; Park et al., 2014). Furthermore, functional BHI may be modulated by signaling occurring, e.g., through pain, viscerceptive, spinothalamocortical, and somatosensory pathways (Bushnell et al., 1999; Craig, 2002; Hofbauer et al., 2001; Khalsa et al., 2009) via biochemical, hormonal, electrical and mechanical changes.

In these regards, the development of computational approaches for the assessment functional BHI, also using task-based experimental paradigms and non-invasive physiological recordings, is of outmost importance (Catrambone and Valenza, 2021a). To this extent, the study of brain-body physiological networks (Antonacci et al., 2020; Pernice et al., 2021), the analysis of spontaneous neural responses to heartbeats (Candia-Rivera et al., 2021d; Petzschner et al., 2019), and the analysis of synchronizations between the brain and heart oscillations (Candia-Rivera et al., 2021d; Pfurtscheller et al., 2018; Valenza et al., 2016, 2020, 2019) have been successfully performed. However, most of the existing methodologies do not take into account the measurement of both ascending heart-to-brain and descending brain-to-heart modulations (Candia-Rivera et al., 2021d). One existing strategy to assess functional BHI, in terms of directionality and modulation time courses, is the model of Synthetic Data Generation (SDG) (Candia-Rivera et al., 2021c; Catrambone et al., 2019), which assesses the bi-directional modulations

Abbreviations: BHI, Brain-heart interplay; SDG, Synthetic data generation; SV-SDG, Sympatho-vagal synthetic data generation; PAI, Parasympathetic activity index; SAI, Sympathetic activity index; ICA, Independent component analysis; MAD, Median absolute deviation; HF, High frequency; LF, Low frequency.

* Corresponding author.
E-mail address: diego.candia.r@ug.uchile.cl (D. Candia-Rivera).

https://doi.org/10.1016/j.neuroimage.2022.119023.
Received 20 October 2021; Received in revised form 16 February 2022; Accepted 18 February 2022
Available online 23 February 2022.

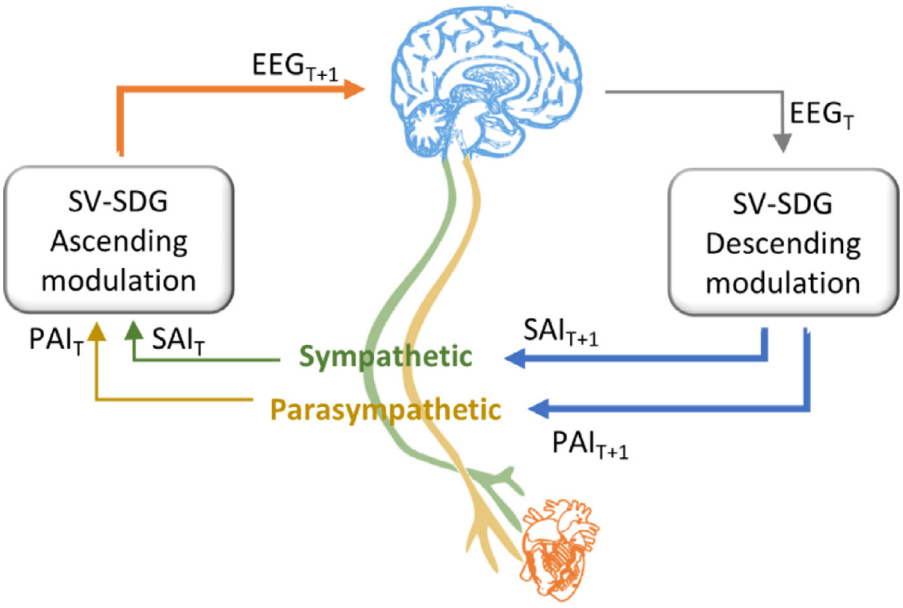

Fig. 1. Sympatho-Vagal Synthetic Data Generation Model (SV-SDG). The model relies on the estimation of autonomous nervous system activity from heart-rate variability, comprising sympathetic (SAI) and parasympathetic (PAI) dynamics. The model assumes a communication loop in which ongoing autonomic activity modulates EEG activity and ongoing EEG activity modulates SAI and PAI.

between EEG oscillations at a given frequency band and heart rate variability spectral estimators for sympathovagal activity. Such model may accurately describe BHI under emotion elicitation (Candia-Rivera et al., 2021c), and shows the potential of physiological modeling for the analysis of BHI. Nevertheless, the study of sympathovagal activity through heart rate's spectral analysis has been challenged because such estimators do not allow a proper quantification of cardiac sympathetic activity. The sympathetic activity is traditionally studied in the 0.04–0.15 Hz range, which present an overlap with parasympathetic oscillations (Reyes del Paso et al., 2013; Valenza et al., 2018a).

To overcome this limitation, here we propose a novel methodology for the assessment of functional BHI, namely the Sympatho-Vagal Synthetic Data Generation (SV-SDG), in which a recursive estimation of heart-to-brain and brain-to-heart interplay is computed (see Fig. 1). The method does not rely on the classical heart-rate's spectral estimators and exploit recent developments on the assessment of peripheral autonomic control: the Sympathetic Activity Index (SAI) and Parasympathetic Activity Index (PAI) (Valenza et al., 2018a). These indices leverage on Laguerre expansions of RR interval series, an alternative mathematical approach to disentangle oscillations, allowing to a personalized decomposition of a signal in slow and fast oscillations, instead of classical Fourier decomposition in sinusoids oscillating in specific frequencies (Mitsis and Marmarelis, 2002). Laguerre expansions can accurately estimate the cardiac sympatho-vagal activity; indeed, SAI and PAI may effectively be used for generating physiologically plausible synthetic heartbeat series (Candia-Rivera et al., 2021b).

In this study, we explore functional BHI changes triggered by the cold-pressor test. Accordingly, we validate our model using data gathered from healthy subjects undergoing thermal stress through a cold-pressor test. Such a thermal stress is known to elicits changes in sympathovagal activity (Cui et al., 2002; Victor et al., 1987), accelerating the heart-rate up to 30 s from the onset (Victor et al., 1987) as a result of an increase in sympathetic activity and decrease in vagal outflow (Mourot et al., 2009). In parallel to the autonomic activity, cortical responses to thermal stress occur within 200 ms (Dowman et al., 2007; Fruhstorfer et al., 1976; Ploner et al., 2006; Wang et al., 2004). EEG studies have reported that these stimuli cause an increase in the power in delta and gamma bands over the fronto-temporal areas (Chang et al., 2002; Fardo et al., 2017; Ferracuti et al., 1994; Huber et al., 2006; Pascalis et al., 2019; Shao et al., 2012; Wang et al., 2020). The existing evidence on functional BHI during thermal stress shows a suppression of heartbeat-evoked potentials (Shao et al., 2011). In addition, BHI models showed a bidirectional interplay with predominant changes through EEG delta and gamma bands, directly related to ascending communication pathways from autonomic inputs (Catrambone et al., 2019).

2. Materials and methods

2.1. Dataset description

A group of 32 right-handed young healthy adults underwent a cold-pressor test while recording physiological signals. Data from 26 subjects (age range 21–41 years, median 27 years, 13 males) were considered in this study for further analysis because of data length and quality. Particularly, data from three subjects were not considered because of the presence of artifacts in their physiological data (EEG or ECG), while data from further three subjects were discarded because of early withdrawal of their hand from the cold water. Each subject recording comprised 128-channel high-density EEG (Electrical Geodesics, Inc.), respiratory activity, and one-lead ECG, sampled at 500 Hz. Before data acquisition, subjects were asked to sit comfortably on a chair to ensure hemodynamic stabilization. The task consisted in a 3 min resting state, followed by up to 3 min cold-pressor test and subsequent recovery, in which subjects were asked to withdraw the hand from the ice water bucket. Throughout the protocol, subjects were asked to keep their eyes closed in order to minimize artifacts. Subjects were guided while submerging their left hand up to their wrist into a bucket filled with ice water (0–4 ˚C).

This study was approved by the local ethical committee Area Vasta Nord-Ovest Toscana. Subjects signed an informed consent to participate in the study, as required by the declaration of Helsinki. All subjects declared no history of neurological, cardiovascular, or respiratory diseases.

2.2. EEG processing

EEG data were pre-processed using MATLAB R2017a and Fieldtrip Toolbox (Oostenveld et al., 2011). Data were bandpass filtered with a Butterworth filter of order 4, between 0.5 and 45 Hz. EEG channels outside the scalp were not considered in this analysis (97 out of the 129 channels were considered), to avoid the interpolation of non-neural data in the correction of contaminated channels detailed below. Large movement artifacts were removed using the wavelet-enhanced independent component analysis (Gabard-Durnam et al., 2018), which were identified using automated thresholding over the independent component and multiplied by a factor of 50 to remove only very large artifacts as

described in (Candia-Rivera et al., 2021d). Consecutively, the Independent Component Analysis (ICA) was re-run to recognize and reject the eye movements and cardiac-field artifacts from the EEG data (Dirlich et al., 1997). To this end, one lead ECG was included as an additional input to the ICA to enhance the process of finding cardiac artifacts. Once the ICA components with eye movements and cardiac artifacts were visually identified, they were set to zero to reconstruct the EEG series. The results of this step were eye-movements and cardiac-artifact-free EEG data. Thus, individual EEG channels were analyzed. The channels were marked as contaminated if their area under the curve exceeded 3 standard deviations of the mean of all channels. The remaining channels were compared with their weighted-by-distance-correlation neighbors using the standard Fieldtrip neighbor's definition. If a channel resulted in a weighted-by-distance correlation of less than 0.6, it was considered contaminated. The contaminated channels were replaced by the neighbor's interpolation. Channels were re-referenced using a common average, which resulted to be the most appropriate for a functional BHI assessment (Candia-Rivera et al., 2021d). Subsequently, a subset of 64 channels (out of 97 channels used until this part) were selected for further analysis to reduce redundancy and to use a standard neighbors' definition in the cluster analysis. The channel selection was performed according to the 10-10 system guidelines (Luu and Ferree, 2000).

The EEG spectrogram was computed using the short-time Fourier transform with a Hanning taper. Calculations were performed through a sliding time window of 2 s with a 50% overlap, resulting in a spectrogram resolution of 1 s and 0.5 Hz. Then, time series were integrated within five frequency bands (delta: 1–4 Hz, theta: 4–8 Hz, alpha: 8–12 Hz, beta: 12–30 Hz, gamma: 30–45 Hz).

2.3. ECG processing

ECG time series were bandpass filtered using a Butterworth filter of order 4, between 0.5 and 45 Hz. The R-peaks from the QRS waves were identified first via an automatized process, followed by a visual inspection of misdetections and final automated correction of remaining misdetections or ectopic heartbeats. The procedure was based on a template-based method for detecting R-peaks (Candia-Rivera et al., 2021d). All the detected peaks were visually inspected over the original ECG, along with the inter-beat intervals histogram. Manual corrections were performed where needed and then automatic corrections were done using a point-process algorithm (Citi et al., 2012).

2.4. Computation of sympathetic and parasympathetic activity indices

The cardiac sympathetic and parasympathetic activities were estimated through Laguerre expansions of the RR interval series, as described in Valenza et al. (2018a). Importantly, this procedure does not require an interpolation of the unevenly sampled RR series, therefore $RR(k)$ indicates the kth sample in time of the original series. The RR series are convolved with a set of Laguerre functions φ_j, as shown in Eq. (1):

$$L_j(k) = \sum_{n=0}^{k-1} \varphi_j(n) \cdot RR(k - n - 1) \tag{1}$$

where n indicates the convolution index of the sum. The RR series can then be expanded using the convolved Laguerre functions $L(k) = [L_0(k),\ L_1(k),\ ...,\ L_8(k)]^T$, and the theoretical autoregressive model can be used to separate the sympathetic and parasympathetic components as follows:

$$RR(k) = \underbrace{g_0(k)}_{baseline} + \underbrace{\sum_{j=0}^{1} g_{1,\,j}(k) \cdot L_j(k)}_{sympathetic} + \underbrace{\sum_{j=2}^{8} g_{1,\,j}(k) \cdot L_j(k)}_{parasympathetic} \tag{2}$$

The time-varying Laguerre coefficients $g(k) = [g_0(k),\ g_{1,\,0}(k),\ ...,\ g_{1,\,8}(k)]^T$ are modelled according to a dynamic system that fulfills Eqs. (3) and (4).

$$g(k) = g(k-1) + \varepsilon_g(k) \tag{3}$$

$$RR(k) = L(k)^T\, g(k) + \varepsilon_{RR}(k) \tag{4}$$

where ε_g is the state noise and ε_{RR} is the observation noise. The coefficients are then estimated using a Kalman filter with a time-varying observation matrix Valenza et al., 2018b), and SAI and PAI are finally estimated as shown in Eqs. (5) and ((6).

$$SAI\ (k) = \left[\Psi s_0 + \sum_{j=1}^{2} \Psi s_j \cdot g_{1,\,j-1}(k)\right] / RR(k) \tag{5}$$

$$PAI\ (k) = \left[\Psi p_0 + \sum_{j=1}^{7} \Psi p_j \cdot g_{1,\,j+1}(k)\right] \cdot 2RR(k) \tag{6}$$

Here, Ψs_j and Ψp_j are the generalized values for the sympathetic and parasympathetic kernels, which were derived from a former selective sympathetic and parasympathetic blockade study; numeric values are $\Psi s_{j\in\{0,1,2\}} = \{39.2343,\ 10.1963,\ -5.9242\}$ and $\Psi p_{j\in\{0,\ldots,7\}} = \{28.4875,\ -17.3627,\ 5.8798,\ 12.0628,\ 5.6408,\ -7.0664,\ -5.6779,\ -3.9474\}$. For a comprehensive description of the model generation and parametrization, see Valenza et al. (2018a). SAI and PAI were computed using a publicly available online software, which can be gathered from www.saipai-hrv.com.

2.5. The proposed Sympatho-Vagal Synthetic Data Generation model

We propose the assessment of functional brain-heart interplay using a model of Sympatho-Vagal Synthetic Data Generation (SV-SDG). The model provides time-variant estimates of the bidirectional coupling coefficients between the different heart and brain components. The source code implementing the SV-SDG model is publicly available at ⟨13:italic ⟩github.com/diegocandiar/brain_heart_svsdg/⟨/13:italic⟩.

2.5.1. Functional interplay from the brain to the heart

The descending interplay is quantified through a physiologically-plausible, synthetic heartbeat generation model leveraging on our recently proposed Sympatho-Vagal Modulation Model (Candia-Rivera et al., 2021b). The synthetic heartbeats are modelled as Dirac functions $\tilde{\delta}(t)$ generating an impulse at the timings of heartbeats occurrences t_k as presented in Eq. (7).

$$x(t) = \sum_{k=1}^{N} \tilde{\delta}(t - t_k) \tag{7}$$

The beat-to-beat generation comprises an integration within the interval from t_k to t_{k+1} on a modulation function of autonomic activity $m(t)$. When the integral function reaches a threshold (equal to 1), the heartbeat is generated, as shown in Eq. (8), where μ_{HR} corresponds to the mean heart rate (in Hz) in the studied interval.

$$1 = \int_{t_k}^{t_{k+1}} \left[\mu_{HR} + m(t)\right] dt \tag{8}$$

The first heartbeat occurs at $t = 0$, and the integration over time is reset to 0 when the threshold is reached. Thus, the model generates heartbeats at a frequency defined by the mean μ_{HR}, whereas the time-varying modulation on the heart rate is defined by the sympathetic and parasympathetic interplay.

Herein, we further implement a sympathovagal modulation model, where heartbeat generation is related to the modulation function *m(t),* which models sympathetic and parasympathetic activities and their respective coupling coefficients with the central nervous system, expressed as C_{SAI} and C_{PAI}:

$$m(t) = C_{SAI}(t) \cdot SAI(t) + C_{PAI}(t) \cdot PAI(t) \tag{9}$$

The model is based on the same hypothesis defined for heartbeat generation in Eqs. (7) and (8). Here, C_{SAI} and C_{PAI} are estimated using a sliding time window and a generalized linear model regression with the constant term omitted for fitting. Regression was performed using a 15 s long time window with a 1 s step. The time series were evenly sampled using a spline interpolation with a 10 Hz sampling frequency, and the resulting RR series data from the model were re-centered to the original mean RR duration.

The model defines the interaction between heartbeat dynamics and the cortical neural control as the ratio between the coupling constants C_{SAI} and C_{PAI} and the EEG power in the previous time window $\mathrm{Power_f}(t-1)$ at a defined frequency f. Therefore, the brain-heart interplay coefficients $\mathrm{SDG_{brain\rightarrow SAI}}$ and $\mathrm{SDG_{brain\rightarrow PAI}}$ are defined by Eqs. (10) and (11), respectively as:

$$\mathrm{SDG_{brain\rightarrow SAI}(t)} = C_{SAI}(t) \,/\, \mathrm{Power_f(t-1)} \tag{10}$$

$$\mathrm{SDG_{brain\rightarrow PAI}(t)} = C_{PAI}(t) \,/\, \mathrm{Power_f(t-1)} \tag{11}$$

2.5.2. Functional interplay from the heart to the brain

The functional interplay from heart to brain is quantified through a model based on the generation of synthetic EEG series using an adaptative Markov process (Al-Nashash et al., 2004), as shown in Eq. (12). The model estimates the modulations to the brain expressed by the coefficient Φ_f using least squares in an auto-regressive process as shown in Eq. (13), where f is the main frequency in a defined frequency band, θ_f is the phase, κ_f is a constant and ε_f is the adjusted error.

$$\mathrm{EEG(t)} = \sum_{f=f_1}^{f_n} \mathrm{Power_f(t)} \cdot \sin\left(\omega_f\, t + \theta_\mathrm{f}\right) \tag{12}$$

$$\mathrm{Power_f(t)} = \kappa_\mathrm{f} \cdot \mathrm{Power_f(t-1)} + \Phi_f(t-1) + \varepsilon_\mathrm{f}, \tag{13}$$

Therefore, the coupling coefficients $\mathrm{SDG_{heart\rightarrow brain}}$ in which the Markovian neural activity generation within a specific EEG channel, frequency band and time window, uses its previous neural activity and heartbeat dynamics as inputs to estimate the contribution of heartbeat dynamics SAI or PAI to the auto-regressive model for EEG data generation:

$$\mathrm{SDG_{SAI\rightarrow brain}(t)} = \Phi_f(t) \,/\, \mathrm{SAI(t)} \tag{14}$$

$$\mathrm{SDG_{PAI\rightarrow brain}(t)} = \Phi_f(t) \,/\, \mathrm{PAI(t)} \tag{15}$$

2.6. Controls on non-stationarities, surrogate data analysis, and confounding factors

Functional BHI coupling coefficients were controlled for the presence of non-stationarities, for the reliability of the estimation through surrogate analysis, and for the presence of confounding respiratory factors.

The analysis for the presence of non-stationarities was inspired by Magagnin et al. (2011). We tested EEG power and heartbeat series for non-stationarity using the so-called Kwiatkowski, Phillips, Schmidt, and Shin (KPSS) test (Hobijn et al., 2004). Series within the interval −60 to 60 s centered to the cold-pressor onset were derived from each subject at each frequency band and were tested as a function of time windows 1–30 s, with 1 s step. Series are associated with a non-stationary process if the p-value from the KPSS test was lower than 0.05, given the null hypothesis of stationarity. In the transition between resting state and cold pressure, series are deemed stationary for length lower than 5 s (see Fig. 5 in Supplementary Material). However, a 15 s estimation window produces reliable results (see Figs. 6 and 7 in Supplementary Material).

We confirmed the reliability of each functional BHI estimation, separately for rest and cold-pressor, through a surrogate data analysis (Porta and Faes, 2016). By considering a rest period from −30 to 0 s with respect to the cold onset and a cold-pressor period from 0 to 30 s with respect to the cold onset, we generated 100 surrogates independently for each EEG power series and SAI/PAI series to preserve first-order moment statistics (average in time) and uncouple brain-heart cross-correlations. The surrogates were generated through random permutations of samples, performed independently for each time series. A p-value was obtained from each estimate (from each subject, channel, direction, autonomic component, and experimental condition) by comparing the original coupling coefficient with respect to a two-tail distribution of coupling coefficients obtained from the surrogate series. Results from a surrogate analysis suggest that more than 50−60% of the estimates were above the significance threshold, which was set to 0.05. We noted that the brain-to-heart functional direction is associated with (10−20%) greater significant estimates than the heart-to-brain direction. Distribution of p-values gathered from EEG series from 4 channels (Fz, Cz, Pz, Oz), for each of the 26 subjects, at 3 EEG frequency bands (delta, alpha, gamma) are shown in Fig. 9 in the Supplementary Material.

Confounding factors as the respiration activity might bias the estimation of autonomic nervous system activity from heart rate variability and, consequently, might bias functional BHI estimates. We estimated the respiratory frequency for each experimental session, i.e., rest and cold-pressor test, by identifying the maximum of the signal frequency spectrum. We confirmed that the main respiratory frequency lies within the HF band (0.15–0.4 Hz) in all the experimental conditions. Because of issues with the belt sensors during the recordings, 16 out of 24 respiratory signals were available for this analysis. Results indicate that the respiratory frequency was non-statistically different between the rest, 0.2056 ± 0.0389 Hz (median ± median absolute deviation), and cold-pressor test, 0.2511 ± 0.0592 Hz (median ± median absolute deviation), with a $p = 0.566$ from a Wilcoxon test for paired samples (see Fig. 8 in the Supplementary Material).

2.7. Statistical analysis

Group-wise statistical analysis between resting state, cold session, and recovery was performed through the non-parametric Friedman test for paired samples. The statistical tests were performed over individual EEG channels, in which the inputs of the Friedman test corresponded to an SV-SDG coupling coefficient computed at different experimental conditions. The significance level of the p-values was corrected in accordance with the Bonferroni rule for 64 channels, with an uncorrected statistical significance set to alpha = 0.05. The samples were described group-wise using the median, and related dispersion measures were expressed as the median absolute deviation (MAD).

Cold-pressure and recovery conditions were compared to the average resting state period with a cluster-based permutation test. The non-parametrical cluster-based permutation tests included a preliminary mask definition, identification of candidate clusters and the computation of cluster statistics with Monte Carlo's p-value correction. The preliminary mask was computed by performing a paired Wilcoxon test for individual samples defined in space, time, and frequency. If a sample obtained a p-value lower than alpha = 0.01, then the sample was considered part of the preliminary mask. Candidate clusters were formed first on individual time stamps and separately for each frequency band. The identification of neighbor channels was based on the default Fieldtrip channels' neighborhood definition for 64 channels. A minimum cluster size of 3 channels was imposed (i.e., one channel needs at least 2 neighbors to form a cluster). Adjacent candidate clusters on time were wrapped if they had at least one channel in common. The overall minimum duration of the cluster was imposed to 5 s. Cluster statistics were computed from 10,000 random partitions. The proportion of random partitions that resulted in a lower p-value than the observed one was considered as the Monte Carlo p-value, with significance at alpha = 0.01. The cluster statistic considered is the Wilcoxon's absolute maximum Z-value obtained from all the samples of the mask.

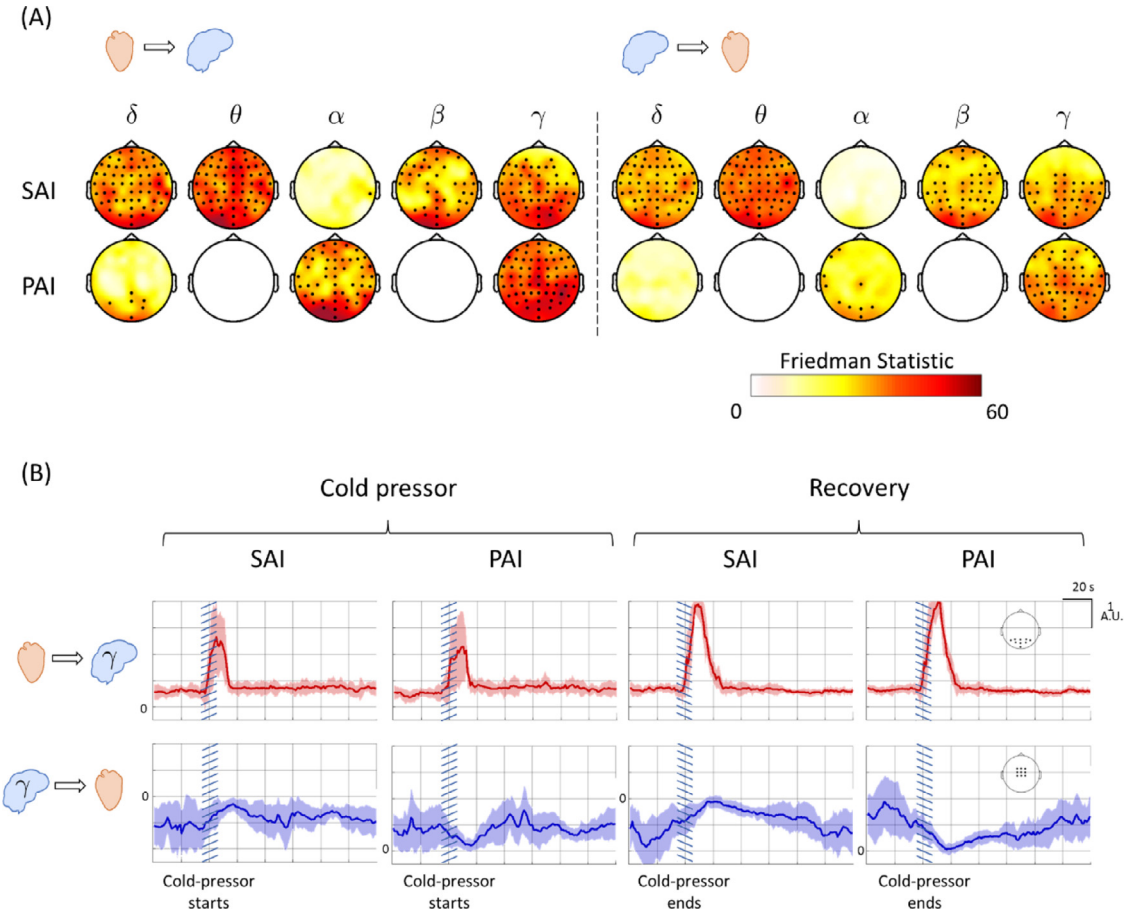

Fig. 2. (A) Results from Friedman tests for heart-to-brain and brain-to-heart interplay from Sympathetic or Parasympathetic Activity Index (SAI or PAI) to EEG frequency bands. The test is performed over 7 phases of the experiment (rest, cold pressor test: 0–20 s, 20–40 s, 40–60 s, and recovery: 0–20 s, 20–40 s, 40–60 s). Colormap represents the Friedman Statistic and thick electrodes represent significant change ($p < 0.05/64$). (B) Exemplary group-wise dynamics related to the bidirectional coupling between SAI/PAI and EEG oscillations in the gamma band over posterior channels (ascending interplay) and central channels (descending interplay) from resting state (40 s before the stimulus onset) to cold-pressor.

3. Results

In this study we applied the SV-SDG model to estimate functional BHI during thermal stress processing, gathered from a hand cold-pressor test. We tested whether the SV-SDG model can uncover the changes in BHI from rest to cold-pressor and recovery. The analysis includes the functional estimation of the bidirectional modulations between sympathovagal activity (SAI and PAI dynamics) and cortical brain oscillations (delta: 1–4 Hz, theta: 4–8 Hz, alpha: 8–12 Hz, beta: 12–30 Hz, gamma: 30–45 Hz).

3.1. Overall changes in functional brain-heart interplay

We first assessed overall changes in functional BHI through the Friedman test, including the conditions of resting state and different latencies from the cold-pressor onset and recovery phases. The ascending modulations from heart to brain showed group-wise changes in a wide scalp coverage (see Fig. 2A), particularly originating from sympathetic activity to EEG delta, theta, beta and gamma oscillations. Ascending modulations from parasympathetic activity was present mostly towards EEG alpha and gamma oscillations.

Sympathetic activity shows a major causal influence on the activity over posterior regions at higher EEG frequency overall midline regions at low EEG frequency. Parasympathetic activity shows major links with the EEG activity from posterior regions over alpha and gamma oscillations. Exemplary time series of the observed BHI changes between EEG gamma oscillations and sympathetic and parasympathetic activity are shown in Fig. 2B. It is possible to observe a rapid change from the ascending interplay lasting approximately 20 s from the cold-pressure onset, along with a decrease in the descending brain-to-heart interplay.

Table 1 shows the estimated functional BHI components associated with a clustered significant change during the cold-pressor phase, with respect to the resting state, within a cluster-based permutation analysis. Note that 120 s corresponds to the minimal duration a subject under cold elicitation. In the ascending direction from the heart-to-brain, the interplay from SAI to delta and theta is suppressed shortly after the phase change; a significant change in the SAI-to-alpha interplay can also be observed. The interplay from brain-to-heart is sustained by sympathetic activity after the phase change, predominantly through delta and gamma oscillations.

3.2. Brain-heart interplay during a phase change

To properly characterize the neural mechanisms associated with the cardiovascular responses to rest-to-cold and cold-to-recovery transitions, here we focus on the observed changes in functional BHI up to 30 s from the phase change onset. To this end, we have performed a cluster-based permutation analysis over the four hypothesized communication pathways: SAI-to-brain, PAI-to-brain, brain-to-SAI and brain-to-PAI throughout the five considered EEG frequency bands. Additionally, we explored the BHI changes measured in the individual brain and heart components.

Table 1
Brain-heart interplay components presenting a clustered effect during the cold-pressor test, and the latency of this change with respect to the cold onset. The interplay changes are assessed in a cluster-based permutation test, compared to the averaged resting state period.

Heart to Brain	latency (s)	*Z*-stat	*p*-value	Brain to Heart	latency (s)	*Z*-stat	*p*-value
SAI→delta	0–21	4.0256	<0.0001	delta→SAI	0–97	3.6446	0.0019
SAI→theta	0–11	3.6446	0.0001	theta→SAI	–	–	–
SAI→alpha	32–59	−3.3652	0.0037	alpha→SAI	–	–	–
SAI→beta	0–113	3.7970	<0.0001	beta→SAI	0–96	3.1367	0.0022
SAI→gamma	0–99	4.3812	<0.0001	gamma→SAI	2–99	3.8478	0.0011
PAI→delta	0–102	4.2542	<0.0001	delta→PAI	–	–	–
PAI→theta	1–76	3.9494	0.0001	theta→PAI	–	–	–
PAI→alpha	–	–	–	alpha→PAI	–	–	–
PAI→beta	0–99	4.2034	<0.0001	beta→PAI	–	–	–
PAI→gamma	0–111	4.4319	<0.0001	gamma→PAI	6–19	−3.1620	0.0061

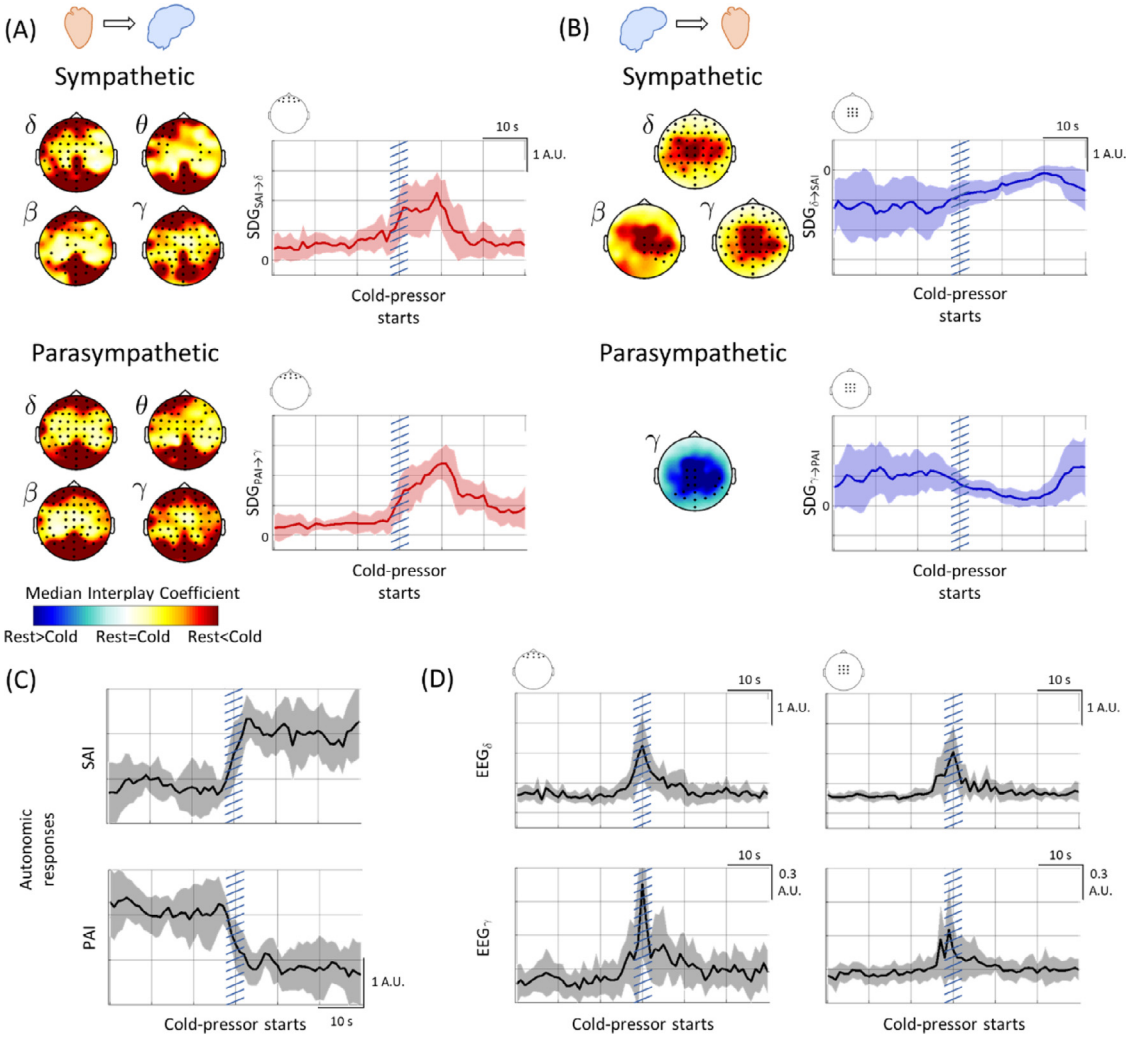

Fig. 3. Brain-Heart Interplay during the cold-pressor test. (A) Ascending heart-to-brain interplay. (B) Descending brain-to-heart interplay. The scalp topographies shown correspond to the components in which significant results were found in the permutation cluster-based analysis. The colorbar represents the group median interplay coefficients, with the resting-state period subtracted. (C) Changes in sympathetic activity (SAI) and parasympathetic activity (PAI). (D) Changes in the EEG power in the delta and gamma bands, in frontal and central electrodes.

Fig. 3A shows the ascending interplay from heart to brain in which significant changes can be observed at the cold-pressor onset. In particular, an increase in the functional BHI is observed at all EEG frequency bands, with the except for the alpha band. The maximum is observed approximately 10 s after the cold-pressor onset. The observed changes are mainly over the midline frontal and posterior regions Fig. 3.B shows the descending interplay from brain to heart, which follows an opposite trend as compared to the ascending interplay. We observed changes only from delta-to-SAI, beta-to-SAI, gamma-to-SAI and gamma-to-PAI. The cold-pressor onset triggers a decrease in the descending interplay absolute value, reaching its minimum in approximately 15–20 s respect the phase change.

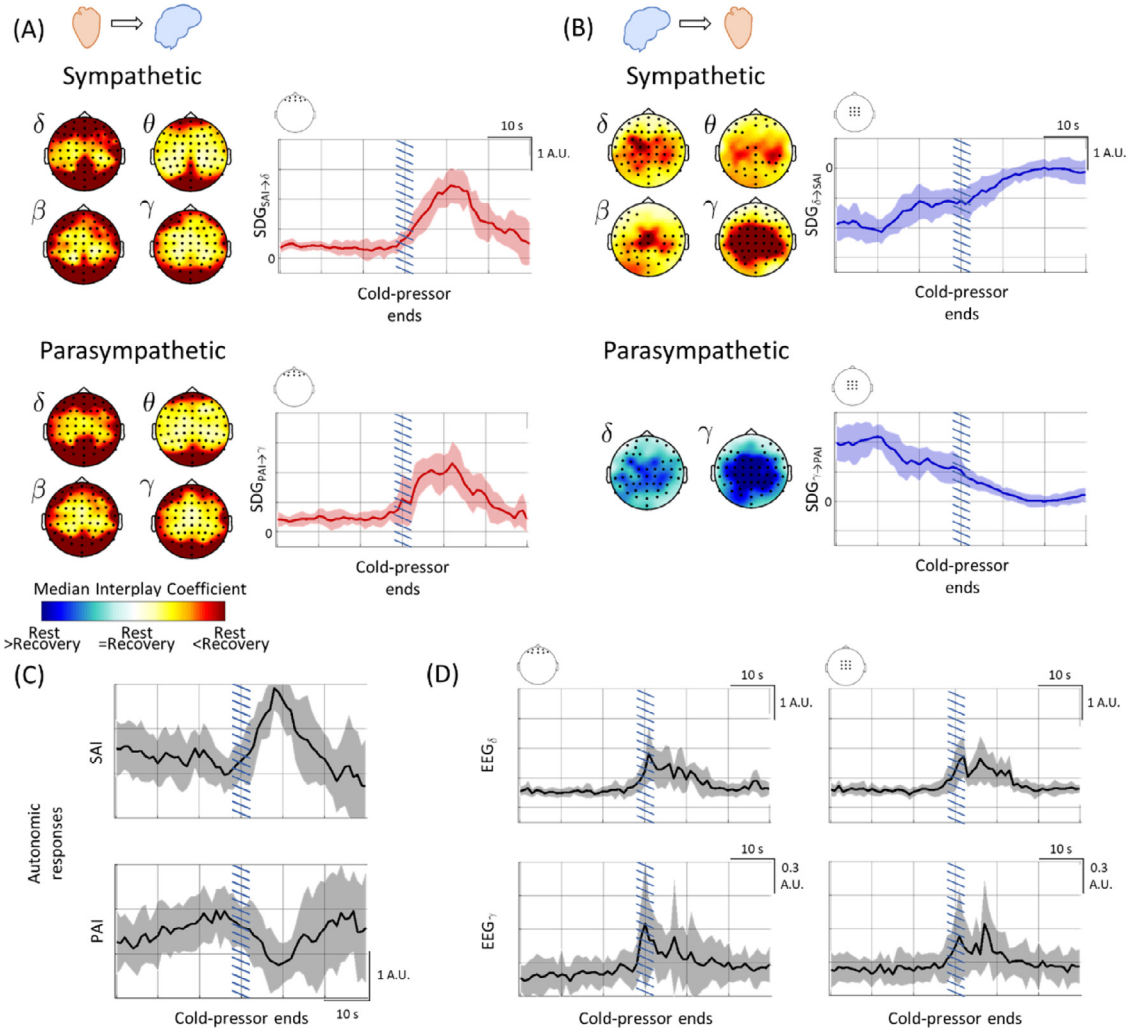

Fig. 4. Brain-Heart Interplay during the recovery from cold-pressor test. (A) Ascending heart-to-brain interplay. (B) Descending brain-to-heart interplay. The scalp topographies shown correspond to the components in which significant results were found in the permutation cluster-based analysis. Colorbar represents the group median interplay coefficients, with the resting-state period subtracted. (C) Changes in sympathetic activity (SAI) and parasympathetic activity (PAI). (D) Changes in the EEG power in the delta and gamma bands, in frontal and central electrodes.

For the sake of completeness, Fig. 3C shows the time course of sympathetic and parasympathetic activity i.e., SAI and PAI, and Fig. 3D shows exemplary EEG activity in the delta and gamma bands. We observe that the cold-pressor triggers an increase in sympathetic activity and EEG power, and a decrease in parasympathetic activity.

The BHI changes observed during the phase change from cold to recovery are similar to the ones observed in the rest-to-cold transition Fig. 4.A shows estimates of the ascending interplay from heart-to-brain. When the cold-pressor ends, a significant increase in the BHI from SAI and PAI to delta, theta, beta and gamma bands is observed over the midline frontal and posterior scalp regions. The cold-pressor offset triggers an increase in the ascending interplay, reaching its maximum after up to 10–15 s with respect to the phase change Fig. 4.B shows the estimates of the descending interplay from the brain-to-heart when the cold-pressor test ends; differently from the cold-pressor onset, changes in the directional interplay between delta-to-SAI, theta-to-SAI, beta-to-SAI, gamma-to-SAI, delta-to-PAI and gamma-to-PAI can be observed. The latencies are slightly delayed from the ascending modulations, reaching the minimum after 15 s from the cold offset.

Fig. 4C shows the time course of sympathetic and parasympathetic activity i.e., SAI and PAI, and Fig. 4D shows exemplary EEG activity in the delta and gamma bands for the recovery transition. The cold-pressor offset triggers an increase in sympathetic activity and a decrease in parasympathetic activity, lasting around 15 s only. Conversely, the EEG power increase lasts longer than the one observed at cold onset, maintaining the relative differences previously observed between lower and higher frequencies.

3.3. Functional brain-heart interplay in recovery mechanisms

In this section we explore the recovery process after the cold offset Table 2. shows the BHI components in which a significant change was observed during the recovery period, with respect to the resting state. In the ascending direction from heart-to-brain, the interplay is suppressed after about 38 s from the phase change. On the functional direction from brain-to-heart, we observe that such a descending interplay is sustained for up to 171 s after the cold offset, with a delay of no less than 11 s with respect to the ascending interplay.

4. Discussion

Computational strategies for a functional BHI assessment aims to quantify the neural information exchange between brain regions and cardiac autonomic control, which occurs through multiple pathways, such as the spino-thalamo-cortical pathway (Craig, 2002). While brain responses to tactile/thermal stimuli or tonic pain have been described

Table 2
Brain-heart interplay components presenting a clustered effect during the recovery period, and the latency of this change with respect to the cold offset. The interplay changes are assessed in a cluster-based permutation test, compared to the averaged resting state period.

Heart to Brain	latency (s)	*Z*-stat	*p*-value	Brain to Heart	latency (s)	*Z*-stat	*p*-value
SAI→delta	0–38	4.4573	<0.0001	delta→SAI	13–171	3.9494	0.0037
SAI→theta	3–21	4.4573	<0.0001	theta→SAI	14–27	3.6192	0.0076
SAI→alpha	123–129	−3.1874	0.0037	alpha→SAI	–	–	–
SAI→beta	3–21	4.4573	<0.0001	beta→SAI	14–46	3.5684	0.004
SAI→gamma	1–25	4.4573	<0.0001	gamma→SAI	11–61	3.7462	0.0005
PAI→delta	0–37	4.4573	<0.0001	delta→PAI	14–171	−3.6446	0.0115
PAI→theta	0–23	4.4573	<0.0001	theta→PAI	–	–	–
PAI→alpha	48–66	−3.4160	0.0008	alpha→PAI	–	–	–
PAI→beta	3–22	4.4573	<0.0001	beta→PAI	16–27	−3.1620	0.0033
PAI→gamma	1–23	4.4573	<0.0001	gamma→PAI	12–62	−3.7970	0.0019

(Bushnell et al., 1999; Hofbauer et al., 2001), there is an important overlap with the described pathways of interoceptive awareness (Craig, 2009, 2002; Khalsa et al., 2009). In this study, building upon existing literature, we explored the functional BHI through the proposed model under sympatho-vagal elicitation driven by a cold-pressor test.

Cortical responses to tactile, thermal, and painful stimuli occur within 200 ms (Dowman et al., 2007; Fruhstorfer et al., 1976; Ploner et al., 2006; Wang et al., 2004), and the initial processing time may last up to 350 ms (Ploner et al., 2006). Subsequent peripheral responses may include heart rate increase within the first 30 s (Victor et al., 1987), as a result of an increase in sympathetic activity and decreased cardiac vagal outflow (Mourot et al., 2009). We found that major changes in brain-heart interplay occur during the first 20 s of the phase change from rest to cold and from cold to recovery, with fewer functional components being involved after that period. Importantly, we found that the transitions from rest to cold-pressure, and cold to no-cold, trigger the ascending interplay first, particularly from the sympathetic activity to primarily midline frontal and posterior scalp regions. Descending interplay, mainly originating over the central regions, occurs with a short delay and lasts 40–100 s. These late autonomic responses to cold pressure of up to 50 s were previously described to be related to feedforward processes (Peng et al., 2015).

The relation between cardiovascular and brain responses to somatosensory stimulation and thermal stress has been previously described through the baroreceptor modulation of heart rate due to physiological arousal (Cui et al., 2002; McIntyre et al., 2006), and heartbeat-evoked potential differences associated with the subjective pain perception (Shao et al., 2011). We showed that the cold-pressor test primarily triggers cardiac sympathetic activity acting towards frontal and posterior cortical regions. Consistently, it was reported that heartbeat-evoked potentials under cold stimuli shows a prominent deflection mainly over the frontal and central scalp locations (Shao et al., 2011). The proposed framework confirmed that the ascending BHI information transfer occurs earlier than the descending one. Indeed, cardiac afferent signals reach subcortical brain areas first, with a subsequent link to higher cortical areas devoted to cardiac afferent information processing (McCraty et al., 2009). In this frame, we recall that pain perception may be modulated by the cardiac cycle (Edwards et al., 2008; Martins et al., 2009), and brain structures involved in the regulation of pain-related responses are linked to perceptual, motor, and autonomic control regions, including the cingulate, medial orbitofrontal and parahippocampal regions (Piché et al., 2010). Moreover, sympathovagal afferent signals from the heart may modulate pain perception through different neural pathways, mediated by the nucleus of tractus solitanus, the periaqueductal gray matter, the thalamus, the hypothalamus, the amygdala, and the prefrontal cortex (McCraty et al., 2009).

Previous studies on EEG correlates of thermal stress and tonic pain showed that the spectral power in the delta-theta range is increased in frontal areas, and power in the beta-gamma range increases as well; the power in the alpha band decreases, with slight differences between studies (Chang et al., 2002; Ferracuti et al., 1994; Huber et al., 2006; Pascalis et al., 2019; Shao et al., 2012; Wang et al., 2020). The scalp regions described in the literature show that fronto-temporal areas are associated with changes in EEG power in the delta-theta and beta-gamma ranges, whereas changes in the alpha band are located over the posterior regions (Chang et al., 2002). Source localizations showed that pain perception was anticorrelated to the power in the theta-alpha range in the prefrontal and cingulate regions, and in the power in the beta band at the posterior-cingulate, temporal, parietal and occipital regions (Shao et al., 2012). In our study, we observed that changes in the delta band were greater than the ones in the gamma band and, at a speculative level, such a difference may be due to an active avoidance process responsible for escape strategies from the cold pain stimuli (Pascalis et al., 2019).

The recovery or post-cold stimuli responses are associated with the so-called reorganization of cerebral electrical activity towards the homeostatic baseline (Chang et al., 2005). In the first 20 s of recovery, BHI dynamics was similar to the one observed right after the cold pressure onset. This suggests that adaptation mechanisms for cold stimuli and its recovery may involve overlapping brain-heart pathways (Chang et al., 2005), at least for the first phases.

Different mechanisms may be employed by the nervous system to ensure an optimal energy use, including anticipation processes in parallel to local feedforward regulatory processes (Sterling, 2012). The multi-process mechanisms observed thanks to our SV-SDG model provide more evidence supporting the role of visceroceptive mechanisms in maintaining homeostasis, as occurs with energy and metabolic control (Quigley et al., 2021).

4.1. On the brain-body communication framework

Brain-body interactions are linked to different neural pathways, including pain and thalamo-cortical pathways (Craig, 2002). Indeed, the thalamo-cortical system and descending inhibitory neuronal networks and the arterial baroreceptor system may be involved in the regulation of pain intensity (Chang et al., 2003; Duschek et al., 2008), as well as contextual changes may influence bodily communications during pain processing (Schwabe et al., 2008). The brain regions including prefrontal/frontal cortex, insular cortex, somatosensory cortex, amygdala, thalamus, hypothalamus, and cingulate cortex, are all involved in interoceptive processing (Cameron, 2009, 2001).

While overlapping brain regions control autonomic pathways for the activity of peripheral organs and systems (e.g., pupil, heart-rate, electro-gastric activity), such regions show also sensory specificity (Rebollo et al., 2018). Indeed, changes in heart rate during cold stimuli depend on the body part under elicitation (Saab et al., 1993). In particular, a functional source separation study showed that scalp frontal responses on EEG to somatosensory hand stimuli are originated in the brainstem, near-thalamic and subthalamic brain regions projecting to the cortex (Gobbelé et al., 2004; Porcaro et al., 2009). The high integration of brain-body communication mechanisms shows the importance

of interoception and homeostasis, and emerging dysfunctions may interfere at a neurological, psychiatric, or behavioral level (Chen et al., 2021).

Previous research has uncovered the involvement of heartbeat dynamics in a number of cognitive processes, including emotions (e.g., Candia-Rivera et al. 2021c, Salamone et al. 2021), mood disorders (Catrambone et al., 2021; Terhaar et al., 2012), self-awareness (Babo-Rebelo et al., 2016; Sel et al., 2017), and consciousness (Candia-Rivera et al., 2021e, 2021a). It has been proposed that the role of the ascending signals, including sympathovagal signaling, may mediate conscious awareness of cognitive and bodily states (Azzalini et al., 2019; Munn et al., 2021). To this extent, experimental evidence has shown that heartbeat dynamics may be involved in shaping somatosensory (Al et al., 2020; Grund et al., 2021), visual (Park et al., 2014), and auditory perceptions (Candia-Rivera et al., 2021e). Likewise, respiration aligns with the perception of sensory inputs, implying that respiration is involved in perceptual sensitivity modulation (Grund et al., 2021; Kluger et al., 2021). Moreover, experimental evidence has shown that cognitive/affective processes modulate physiological responses to cold and pain (Rainville et al., 2005; Rhudy et al., 2007; Santarcangelo et al., 2013), and the somatization of emotions in the body (Nummenmaa et al., 2018). Further evidence in this regard shows differences between resting state and mental arithmetic performance, in which the effects of the physiological arousal level was inhibited according to the cardiac cycle during rest only (McIntyre et al., 2006). Similarly, the evidence on heartbeat-evoked potentials during cold stimuli showed significant changes in BHI, but this effect was minimized when subjects performed mental calculations (Shao et al., 2011). Previous research on thermal stress has shown effects on memory as well (Duncko et al., 2009; Ishizuka et al., 2007). EEG studies showed changes in the alpha band, which is repeatedly interpreted as a possible reflect of the increased attention related to the processing of stimuli, with a consecutive inverse effect to motivation (Chang et al., 2002; Dowman et al., 2008). Those effects were later confirmed in a task of controlled attention levels (Giehl et al., 2014). In our study, we observed that BHI changes involving EEG oscillations in the alpha band were not triggered by the change in the experimental condition, in line with the interpretation above. In this context, the dominance of resting background or idling activity associated with the cold-pressor test might have played a role. Further investigation is needed to demonstrate if these observed changes may be related to either a direct effect of thermal stress, or changes in attention or arousal, or possibly to an unspecified indirect cause mediated in part by BHI.

4.2. Clinical relevance

The understanding of the role of BHI is of importance in several clinical domains (Chen et al., 2021). A variety of clinical evidence exists on pathological conditions and disrupted BHI (Catrambone and Valenza, 2021b; Critchley, 2005; Critchley et al., 2005, 2003; Tahsili-Fahadan and Geocadin, 2017). Indeed, the characterization of functional BHI has contributed to the development of novel biomarkers with potential clinical use (Candia-Rivera et al., 2021a; Catrambone et al., 2021; Iseger et al., 2021; Perogamvros et al., 2019; Schiecke et al., 2019; Terhaar et al., 2012). Such a clinical relevance is also supported by the so-called human neurovisceral integration, showing changes after vagus nerve stimulation on interoception (Richter et al., 2020), and reinforcement learning (Weber et al., 2021), as well as the changes in cardiac interoception after heart transplant (Salamone et al., 2020). Further clinical applications include the control of anesthetics, given that cardiac markers have shown features assessing analgesia (Jeanne et al., 2009), and, importantly, a better understanding of the role of the heart in these mechanisms could explain the existing relations between the use of general anesthesia and worsen patients' outcomes after stroke (Campbell et al., 2018).

4.3. Limitations and future directions of the research

The proposed study effectively provides novel quantitative BHI measurements. However, we are aware that many aspects, such as the low time resolution given the EEG spectral representation and the estimation of the SV-SDG coefficients using a sliding time window, should be improved in future endeavors. The specific model of the interplay between brain and heart is a peculiar aspect of the proposed methodology. Given the complexity of such an interplay, we did not follow specific physiological considerations, but rather considered the simplest non-trivial coupling between dynamical system: the linear bidirectional coupling. The rationale underlying this formulation is that the activity of one interacting system (e.g., sympathetic activity for cardiovascular dynamics) is proportionally modulated by activity of the other system (e.g., α power desynchronization for brain dynamics). Moreover, the proposed model does not account for autonomic covariates as respiratory activity, blood pressure, and others. In addition, further investigations on BHI mechanisms should be directed toward the assessment of interoceptive mechanisms in cognitive states, as observed in heartbeat-evoked potentials and the links to the cardiac cycle (McIntyre et al., 2006; Shao et al., 2011). Indeed, much more remains to be uncovered on the specific physiological and anatomical mechanisms that allow transfer of information from neural responses at any level in the brain and autonomic modulation of the heart.

5. Conclusion

The proposed SV-SDG modeling has successfully been applied for the assessment of for a functional and causal BHI (ascending heart-to-brain and descending brain-to-heart interplay) during thermal stress. The advantages of assessing directionality and latencies of functional BHI are numerous in the neuroscientific and clinical domains. Importantly, for the first time, the proposed methodology highlights cardiac sympathetic and vagal activities sustaining cortical dynamics.

Glossary

$\tilde{\delta}$: Dirac delta
ε_{f}: Error to adjust modeling at frequency f
ε_g: state noise
ε_{RR}: observation noise
θ_{f}: Phase frequency f
κ_{f}: Constant to adjust modeling at frequency f
μV: micro volts
μ_{HR}: mean heart rate (Hz)
φ_j: Laguerre function of order j
Φ_f: Increase of EEG power at frequency f
Ψp_j: Generalized values of parasympathetic kernels of order j
Ψs_j: Generalized values of sympathetic kernels of order j
ω_f: Frequency (rad/s)
C_{PAI}: Time-varying coefficients of central modulation to parasympathetic activity
C_{SAI}: Time-varying coefficients of central modulation to sympathetic activity
g_j: Laguerre coefficients of the Laguerre function of order j
L_j: Convolved Laguerre function of order j
$m(t)$: Heart modulation function
PAI: Parasympathetic activity index (arbitrary units)
$\mathrm{Power}_{\mathrm{f}}$: EEG power measured at the frequency f (μV^2/Hz)
RR: R-to-R interval duration (seconds)
SAI: Sympathetic activity index (arbitrary units)
SDG: Synthetic Data Generation
$\mathrm{SDG}_{\mathrm{brain}\rightarrow\mathrm{PAI}}$: Time-varying coefficients measuring brain to PAI interplay
$\mathrm{SDG}_{\mathrm{brain}\rightarrow\mathrm{SAI}}$: Time-varying coefficients measuring brain to SAI interplay

$SDG_{PAI \rightarrow brain}$: Time-varying coefficients measuring PAI to brain interplay

$SDG_{SAI \rightarrow brain}$: Time-varying coefficients measuring SAI to brain interplay

SV – SDG: Sympathovagal Synthetic Data Generation

$x(t)$: modelled ECG as a sum of impulse trains

Disclosures

Authors declare no competing interests.

Data and code availability statement

Data is available upon reasonable request. Codes and software are freely available online as detailed in Material and methods section

Credit authorship contribution statement

Diego Candia-Rivera: Methodology, Visualization, Data curation, Formal analysis, Writing – review & editing. **Vincenzo Catrambone:** Methodology, Formal analysis, Writing – review & editing. **Riccardo Barbieri:** Formal analysis, Writing – review & editing. **Gaetano Valenza:** Visualization, Formal analysis, Writing – review & editing.

Acknowledgment

The research leading to these results has received partial funding from the European Commission - Horizon 2020 Program under grant agreement no. 813234 of the project “RHUMBO”, and from the Italian Ministry of Education and Research (MIUR) in the framework of the CrossLab project (Departments of Excellence).

Supplementary materials

Supplementary material associated with this article can be found, in the online version, at doi:10.1016/j.neuroimage.2022.119023.

References

Al, E., Iliopoulos, F., Forschack, N., Nierhaus, T., Grund, M., Motyka, P., Gaebler, M., Nikulin, V.V., Villringer, A., 2020. Heart–brain interactions shape somatosensory perception and evoked potentials. Proc. Natl. Acad. Sci. 117, 10575–10584. doi:10.1073/pnas.1915629117.

Al-Nashash, H., Al-Assaf, Y., Paul, J., Thakor, N., 2004. EEG signal modeling using adaptive Markov process amplitude. IEEE Trans. Biomed. Eng. 51, 744–751. doi:10.1109/TBME.2004.826602.

Antonacci, Y., Astolfi, L., Nollo, G., Faes, L., 2020. Information transfer in linear multivariate processes assessed through penalized regression techniques: validation and application to physiological networks. Entropy 22, 732. doi:10.3390/e22070732.

Azzalini, D., Rebollo, I., Tallon-Baudry, C., 2019. Visceral signals shape brain dynamics and cognition. Trends Cogn. Sci. 23, 488–509. doi:10.1016/j.tics.2019.03.007, (Regul. Ed.).

Babo-Rebelo, M., Richter, C.G., Tallon-Baudry, C., 2016. Neural responses to heartbeats in the default network encode the self in spontaneous thoughts. J. Neurosci. 36, 7829–7840. doi:10.1523/JNEUROSCI.0262-16.2016.

Blanke, O., Metzinger, T., 2009. Full-body illusions and minimal phenomenal selfhood. Trends Cogn. Sci. 13, 7–13. doi:10.1016/j.tics.2008.10.003, (Regul. Ed.).

Bushnell, M.C., Duncan, G.H., Hofbauer, R.K., Ha, B., Chen, J.-.I., Carrier, B., 1999. Pain perception: is there a role for primary somatosensory cortex? Proc. Natl. Acad. Sci. 96, 7705–7709. doi:10.1073/pnas.96.14.7705.

Cameron, O.G., 2009. Visceral brain–body information transfer. NeuroImage 47, 787–794. doi:10.1016/j.neuroimage.2009.05.010, Brain Body Medicine.

Cameron, O.G., 2001. Interoception: the inside story—a model for psychosomatic processes. Psychosom. Med. 63, 697–710.

Campbell, B.C.V., et al., 2018. Effect of general anaesthesia on functional outcome in patients with anterior circulation ischaemic stroke having endovascular thrombectomy versus standard care: a meta-analysis of individual patient data. The Lancet Neurol. 17, 47–53. doi:10.1016/S1474-4422(17)30407-6.

Candia-Rivera, D., Annen, J., Gosseries, O., Martial, C., Thibaut, A., Laureys, S., Tallon-Baudry, C., 2021a. Neural responses to heartbeats detect residual signs of consciousness during resting state in postcomatose patients. J. Neurosci. 41, 5251–5262. doi:10.1523/JNEUROSCI.1740-20.2021.

Candia-Rivera, D., Catrambone, V., Barbieri, R., Valenza, G., 2021b. Integral pulse frequency modulation model driven by sympathovagal dynamics: synthetic vs. real heart rate variability. Biomed. Signal Process. Control 68, 102736. doi:10.1016/j.bspc.2021.102736.

Candia-Rivera, D., Catrambone, V., Thayer, J.F., Gentili, C., Valenza, G., 2021c. Cardiac sympathovagal activity initiates a functional brain-body response to emotional processing. bioRxiv doi:10.1101/2021.06.05.447188, 2021.06.05.447188.

Candia-Rivera, D., Catrambone, V., Valenza, G., 2021d. The role of electroencephalography electrical reference in the assessment of functional brain–heart interplay: from methodology to user guidelines. J. Neurosci. Methods 360, 109269. doi:10.1016/j.jneumeth.2021.109269.

Candia-Rivera, D., Raimondo, F., Perez, P., Naccache, L., Tallon-Baudry, C., Sitt, J.D., 2021e. Processing of slow-global auditory regularities causes larger neural responses to heartbeats in patients under minimal consciousness state, compared to unresponsive wakefulness syndrome. medRxiv, 10.1101/2021.10.27.21265539; doi:10.1101/2021.10.27.21265539.

Catrambone, V., Greco, A., Vanello, N., Scilingo, E.P., Valenza, G., 2019. Time-resolved directional brain-heart interplay measurement through synthetic data generation models. Ann. Biomed. Eng. 47, 1479–1489. doi:10.1007/s10439-019-02251-y.

Catrambone, V., Messerotti Benvenuti, S., Gentili, C., Valenza, G., 2021. Intensification of functional neural control on heartbeat dynamics in subclinical depression. Transl. Psychiatry 11, 1–10. doi:10.1038/s41398-021-01336-4.

Catrambone, V., Valenza, G., 2021a. BHI estimation methodology. In: Catrambone, V., Valenza, G. (Eds.), Functional Brain-Heart Interplay: From Physiology to Advanced Methodology of Signal Processing and Modeling. Springer International Publishing, Cham, pp. 21–50. doi:10.1007/978-3-030-79934-2_2.

Catrambone, V., Valenza, G., 2021b. Psychiatric and neurological disorders. In: Catrambone, V., Valenza, G. (Eds.), Functional Brain-Heart Interplay: From Physiology to Advanced Methodology of Signal Processing and Modeling. Springer International Publishing, Cham, pp. 117–141. doi:10.1007/978-3-030-79934-2_5.

Chang, P.F., Arendt-Nielsen, L., Chen, A.C.N., 2005. Comparative cerebral responses to non-painful warm vs. cold stimuli in man: EEG power spectra and coherence. Int. J. Psychophysiol. 55, 73–83. doi:10.1016/j.ijpsycho.2004.06.006.

Chang, P.F., Arendt-Nielsen, L., Chen, A.C.N., 2002. Dynamic changes and spatial correlation of EEG activities during cold pressor test in man. Brain Res. Bull. 57, 667–675. doi:10.1016/S0361-9230(01)00763-8.

Chang, P.F., Arendt-Nielsen, L., Graven-Nielsen, T., Chen, A.C.N., 2003. Psychophysical and EEG responses to repeated experimental muscle pain in humans: pain intensity encodes EEG activity. Brain Res. Bull. 59, 533–543. doi:10.1016/S0361-9230(02)00950-4.

Chen, W.G., Schloesser, D., Arensdorf, A.M., Simmons, J.M., Cui, C., Valentino, R., Gnadt, J.W., Nielsen, L., Hillaire-Clarke, C.St., Spruance, V., Horowitz, T.S., Vallejo, Y.F., Langevin, H.M., 2021. The Emerging science of interoception: sensing, integrating, interpreting, and regulating signals within the self. Trends Neurosci. 44, 3–16. doi:10.1016/j.tins.2020.10.007, Special Issue: The Neuroscience of Interoception.

Citi, L., Brown, E.N., Barbieri, R., 2012. A real-time automated point process method for detection and correction of erroneous and ectopic heartbeats. IEEE Trans. Biomed. Eng. 59, 2828–2837. doi:10.1109/TBME.2012.2211356.

Craig, A.D., 2009. How do you feel — now? The anterior insula and human awareness. Nat. Rev. Neurosci. 10, 59–70. doi:10.1038/nrn2555.

Craig, A.D., 2002. How do you feel? Interoception: the sense of the physiological condition of the body. Nat. Rev. Neurosci. 3, 655–666. doi:10.1038/nrn894.

Critchley, H.D., 2005. Neural mechanisms of autonomic, affective, and cognitive integration. J. Comp. Neurol. 493, 154–166. doi:10.1002/cne.20749.

Critchley, H.D., Harrison, N.A., 2013. Visceral influences on brain and behavior. Neuron 77, 624–638. doi:10.1016/j.neuron.2013.02.008.

Critchley, H.D., Mathias, C.J., Josephs, O., O'Doherty, J., Zanini, S., Dewar, B.K., Cipolotti, L., Shallice, T., Dolan, R.J., 2003. Human cingulate cortex and autonomic control: converging neuroimaging and clinical evidence. Brain 126, 2139–2152. doi:10.1093/brain/awg216.

Critchley, H.D., Taggart, P., Sutton, P.M., Holdright, D.R., Batchvarov, V., Hnatkova, K., Malik, M., Dolan, R.J., 2005. Mental stress and sudden cardiac death: asymmetric midbrain activity as a linking mechanism. Brain 128, 75–85. doi:10.1093/brain/awh324.

Cui, J., Wilson, T.E., Crandall, C.G., 2002. Baroreflex modulation of muscle sympathetic nerve activity during cold pressor test in humans. Am. J. Physiol. Heart Circ. Physiol. 282, H1717–H1723. doi:10.1152/ajpheart.00899.2001.

Dirlich, G., Vogl, L., Plaschke, M., Strian, F., 1997. Cardiac field effects on the EEG. Electroencephalogr. Clin. Neurophysiol. 102, 307–315. doi:10.1016/S0013-4694(96)96506-2.

Dowman, R., Darcey, T., Barkan, H., Thadani, V., Roberts, D., 2007. Human intracranially-recorded cortical responses evoked by painful electrical stimulation of the sural nerve. Neuroimage 34, 743–763. doi:10.1016/j.neuroimage.2006.09.021.

Dowman, R., Rissacher, D., Schuckers, S., 2008. EEG indices of tonic pain-related activity in the somatosensory cortices. Clin. Neurophysiol. 119, 1201–1212. doi:10.1016/j.clinph.2008.01.019.

Duncko, R., Johnson, L., Merikangas, K., Grillon, C., 2009. Working memory performance after acute exposure to the cold pressor stress in healthy volunteers. Neurobiol. Learn. Mem. 91, 377–381. doi:10.1016/j.nlm.2009.01.006.

Duschek, S., Schwarzkopf, W., Schandry, R., 2008. Increased pain sensitivity in low blood pressure. J. Psychophysiol. 22, 20–27. doi:10.1027/0269-8803.22.1.20.

Edwards, L., Inui, K., Ring, C., Wang, X., Kakigi, R., 2008. Pain-related evoked potentials are modulated across the cardiac cycle. PAIN® 137, 488–494. doi:10.1016/j.pain.2007.10.010.

Fardo, F., Vinding, M.C., Allen, M., Jensen, T.S., Finnerup, N.B., 2017. Delta and gamma oscillations in operculo-insular cortex underlie innocuous cold thermosensation. J. Neurophysiol. 117, 1959–1968. doi:10.1152/jn.00843.2016.

Ferracuti, S., Seri, S., Mattia, D., Cruccu, G., 1994. Quantitative EEG modifications during the cold water pressor test: hemispheric and hand differences. Int. J. Psychophysiol. 17, 261–268. doi:10.1016/0167-8760(94)90068-X.

Fruhstorfer, H., Guth, H., Pfaff, U., 1976. Cortical responses evoked by thermal stimuli in man. In: McCallum, W.C., Knott, J.R. (Eds.), The Responsive Brain. Butterworth-Heinemann, pp. 30–33. doi:10.1016/B978-0-7236-0443-3.50013-1.

Gabard-Durnam, L.J., Mendez Leal, A.S., Wilkinson, C.L., Levin, A.R., 2018. The Harvard Automated Processing Pipeline for Electroencephalography (HAPPE): standardized processing software for developmental and high-artifact data. Front. Neurosci. 12. doi:10.3389/fnins.2018.00097.

Giehl, J., Meyer-Brandis, G., Kunz, M., Lautenbacher, S., 2014. Responses to tonic heat pain in the ongoing EEG under conditions of controlled attention. Somatosens. Mot. Res. 31, 40–48. doi:10.3109/08990220.2013.837045.

Gobbelé, R., Waberski, T.D., Simon, H., Peters, E., Klostermann, F., Curio, G., Buchner, H., 2004. Different origins of low- and high-frequency components (600Hz) of human somatosensory evoked potentials. Clin. Neurophysiol. 115, 927–937. doi:10.1016/j.clinph.2003.11.009.

Grund, M., Al, E., Pabst, M., Dabbagh, A., Stephani, T., Nierhaus, T., Gaebler, M., Villringer, A., 2021. Respiration, heartbeat, and conscious tactile perception. J. Neurosci. doi:10.1523/JNEUROSCI.0592-21.2021.

Hobijn, B., Franses, P.H., Ooms, M., 2004. Generalizations of the KPSS-test for stationarity. Stat. Neerl. 58, 483–502. doi:10.1111/j.1467-9574.2004.00272.x.

Hofbauer, R.K., Rainville, P., Duncan, G.H., Bushnell, M.C., 2001. Cortical representation of the sensory dimension of pain. J. Neurophysiol. 86, 402–411. doi:10.1152/jn.2001.86.1.402.

Huber, M.T., Bartling, J., Pachur, D., Woikowsky-Biedau, S.V., Lautenbacher, S., 2006. EEG responses to tonic heat pain. Exp. Brain Res. 173, 14–24. doi:10.1007/s00221-006-0366-1.

Iseger, T.A., Padberg, F., Kenemans, J.L., van Dijk, H., Arns, M., 2021. Neuro-Cardiac-Guided TMS (NCG TMS): a replication and extension study. Biol. Psychol. 162, 108097. doi:10.1016/j.biopsycho.2021.108097.

Ishizuka, K., Hillier, A., Beversdorf, D.Q., 2007. Effect of the cold pressor test on memory and cognitive flexibility. Neurocase 13, 154–157. doi:10.1080/13554790701441403.

Jeanne, M., Logier, R., De Jonckheere, J., Tavernier, B., 2009. Heart rate variability during total intravenous anesthesia: effects of nociception and analgesia. Auton. Neurosci. 147, 91–96. doi:10.1016/j.autneu.2009.01.005.

Khalsa, S.S., Rudrauf, D., Feinstein, J.S., Tranel, D., 2009. The pathways of interoceptive awareness. Nat. Neurosci. 12, 1494–1496. doi:10.1038/nn.2411.

Kluger, D.S., Balestrieri, E., Busch, N.A., Gross, J., 2021. Respiration aligns perception with neural excitability. eLife 10, e70907. doi:10.7554/eLife.70907.

Luu, P., Ferree, T.C., 2000. Determination of the geodesic sensor nets' average electrode positions and their 10–10 international equivalents. OR: Electrical Geodesics, Eugene.

Magagnin, V., Bassani, T., Bari, V., Turiel, M., Maestri, R., Pinna, G.D., Porta, A., 2011. Non-stationarities significantly distort short-term spectral, symbolic and entropy heart rate variability indices. Physiol. Meas. 32, 1775–1786. doi:10.1088/0967-3334/32/11/S05.

Martins, A.Q., Ring, C., McIntyre, D., Edwards, L., Martin, U., 2009. Effects of unpredictable stimulation on pain and nociception across the cardiac cycle. PAIN® 147, 84–90. doi:10.1016/j.pain.2009.08.016.

McCraty, R., Mike, A., Tomasino, D., Bradley, R., 2009. The coherent heart heart–brain interactions, psychophysiological coherence, and the emergence of system-wide order. Integral Rev. 5.

McIntyre, D., Edwards, L., Ring, C., Parvin, B., Carroll, D., 2006. Systolic inhibition of nociceptive responding is moderated by arousal. Psychophysiology 43, 314–319. doi:10.1111/j.1469-8986.2006.00407.x.

Mitsis, G.D., Marmarelis, V.Z., 2002. Modeling of nonlinear physiological systems with fast and slow dynamics. I. Methodology. Ann. Biomed. Eng. 30, 272–281. doi:10.1114/1.1458591.

Mourot, L., Bouhaddi, M., Regnard, J., 2009. Effects of the cold pressor test on cardiac autonomic control in normal subjects. Physiol. Res. 58, 83–91.

Munn, B.R., Müller, E.J., Wainstein, G., Shine, J.M., 2021. The ascending arousal system shapes neural dynamics to mediate awareness of cognitive states. Nat. Commun. 12, 6016. doi:10.1038/s41467-021-26268-x.

Nummenmaa, L., Hari, R., Hietanen, J.K., Glerean, E., 2018. Maps of subjective feelings. Proc. Natl. Acad. Sci. 115, 9198–9203. doi:10.1073/pnas.1807390115.

Oostenveld, R., Fries, P., Maris, E., Schoffelen, J.M., 2011. FieldTrip: open source software for advanced analysis of MEG, EEG, and invasive electrophysiological data. Comput. Intell. Neurosci. 9. doi:10.1155/2011/156869, 2011pages.

Park, H.D., Bernasconi, F., Bello-Ruiz, J., Pfeiffer, C., Salomon, R., Blanke, O., 2016. Transient modulations of neural responses to heartbeats covary with bodily self-consciousness. J. Neurosci. 36, 8453–8460. doi:10.1523/JNEUROSCI.0311-16.2016.

Park, H.D., Correia, S., Ducorps, A., Tallon-Baudry, C., 2014. Spontaneous fluctuations in neural responses to heartbeats predict visual detection. Nat. Neurosci. 17, 612–618. doi:10.1038/nn.3671.

Pascalis, V.D., Scacchia, P., Papi, B., Corr, P.J., 2019. Changes of EEG band oscillations to tonic cold pain and the behavioral inhibition and fight-flight-freeze systems. Personal. Neurosci. 2. doi:10.1017/pen.2019.9.

Peng, R.C., Yan, W.R., Zhou, X.L., Zhang, N.L., Lin, W.H., Zhang, Y.T., 2015. Time-frequency analysis of heart rate variability during the cold pressor test using a time-varying autoregressive model. Physiol. Meas. 36, 441–452. doi:10.1088/0967-3334/36/3/441.

Pernice, R., Antonacci, Y., Zanetti, M., Busacca, A., Marinazzo, D., Faes, .L.., Nollo, G., 2021. Multivariate correlation measures reveal structure and strength of brain–body physiological networks at rest and during mental stress. Front. Neurosci. 14, 1427. doi:10.3389/fnins.2020.602584.

Perogamvros, L., Park, H.D., Bayer, L., Perrault, A.A., Blanke, O., Schwartz, S., 2019. Increased heartbeat-evoked potential during REM sleep in nightmare disorder. NeuroImage Clin. 22, 101701. doi:10.1016/j.nicl.2019.101701.

Petzschner, F.H., Weber, L.A., Wellstein, K.V., Paolini, G., Do, C.T., Stephan, K.E., 2019. Focus of attention modulates the heartbeat evoked potential. Neuroimage 186, 595–606. doi:10.1016/j.neuroimage.2018.11.037.

Pfurtscheller, G., Schwerdtfeger, A., Seither-Preisler, A., Brunner, C., Aigner, C.S., Calisto, J., Gens, J., Andrade, A., 2018. Synchronization of intrinsic 0.1-Hz blood-oxygen-level-dependent oscillations in amygdala and prefrontal cortex in subjects with increased state anxiety. Eur. J. Neurosci. 47, 417–426. doi:10.1111/ejn.13845.

Piché, M., Arsenault, M., Rainville, P., 2010. Dissection of perceptual, motor and autonomic components of brain activity evoked by noxious stimulation. Pain 149, 453–462. doi:10.1016/j.pain.2010.01.005.

Ploner, M., Gross, J., Timmermann, L., Schnitzler, A., 2006. Pain processing is faster than tactile processing in the human brain. J. Neurosci. 26, 10879–10882. doi:10.1523/JNEUROSCI.2386-06.2006.

Porcaro, C., Coppola, G., Lorenzo, G.D., Zappasodi, F., Siracusano, A., Pierelli, F., Rossini, P.M., Tecchio, F., Seri, S., 2009. Hand somatosensory subcortical and cortical sources assessed by functional source separation: an EEG study. Hum. Brain Mapp. 30, 660–674. doi:10.1002/hbm.20533.

Porta, A., Faes, L., 2016. Wiener–granger causality in network physiology with applications to cardiovascular control and neuroscience. Proc. IEEE 104, 282–309. doi:10.1109/JPROC.2015.2476824.

Quigley, K.S., Kanoski, S., Grill, W.M., Barrett, L.F., Tsakiris, M., 2021. Functions of interoception: from energy regulation to experience of the self. Trends Neurosci. 44, 29–38. doi:10.1016/j.tins.2020.09.008, Special Issue: The Neuroscience of Interoception.

Rainville, P., Bao, Q.V.H., Chrétien, P., 2005. Pain-related emotions modulate experimental pain perception and autonomic responses. Pain 118, 306–318. doi:10.1016/j.pain.2005.08.022.

Rebollo, I., Devauchelle, A.D., Béranger, B., Tallon-Baudry, C., 2018. Stomach-brain synchrony reveals a novel, delayed-connectivity resting-state network in humans. eLife 7, e33321. doi:10.7554/eLife.33321.

Reyes del Paso, G.A., Langewitz, W., Mulder, L.J.M., van Roon, A., Duschek, S., 2013. The utility of low frequency heart rate variability as an index of sympathetic cardiac tone: a review with emphasis on a reanalysis of previous studies. Psychophysiology 50, 477–487. doi:10.1111/psyp.12027.

Rhudy, J.L., McCabe, K.M., Williams, A.E., 2007. Affective modulation of autonomic reactions to noxious stimulation. Int. J. Psychophysiol. 63, 105–109. doi:10.1016/j.ijpsycho.2006.09.001.

Richter, F., García, A.M., Arriagada, N.R., Yoris, A., Birba, A., Huepe, D., Zimmer, H., Ibáñez, A., Sedeño, L., 2020. Behavioral and neurophysiological signatures of interoceptive enhancements following vagus nerve stimulation. Hum. Brain Mapp. doi:10.1002/hbm.25288, n/a.

Saab, P.G., Llabre, M.M., Hurwitz, B.E., Schneiderman, N., Wohlgemuth, W., Durel, L.A., Massie, C., Nagel, J., 1993. The cold pressor test: vascular and myocardial response patterns and their stability. Psychophysiology 30, 366–373. doi:10.1111/j.1469-8986.1993.tb02058.x.

Salamone, P.C., Legaz, A., Sedeño, L., Moguilner, S., Fraile-Vazquez, M., Campo, C.G., Fittipaldi, S., Yoris, A., Miranda, M., Birba, A., Galiani, A., Abrevaya, S., Neely, A., Caro, M.M., Alifano, F., Villagra, R., Anunziata, F., Oliveira, M.O.de, Pautassi, R.M., Slachevsky, A., Serrano, C., García, A.M., Ibañez, A., 2021. Interoception primes emotional processing: multimodal evidence from neurodegeneration. J. Neurosci. 41, 4276–4292. doi:10.1523/JNEUROSCI.2578-20.2021.

Salamone, P.C., Sedeño, L., Legaz, A., Bekinschtein, T., Martorell, M., Adolfi, F., Fraile-Vazquez, M., Rodríguez Arriagada, N., Favaloro, L., Peradejordi, M., Absi, D.O., García, A.M., Favaloro, R., Ibáñez, A., 2020. Dynamic neurocognitive changes in interoception after heart transplant. Brain Commun. 2. doi:10.1093/braincomms/fcaa095.

Santarcangelo, E.L., Paoletti, G., Chiavacci, I., Palombo, C., Carli, G., Varanini, M., 2013. Cognitive modulation of psychophysical, respiratory and autonomic responses to cold pressor test. PLoS One 8, e75023. doi:10.1371/journal.pone.0075023.

Schiecke, K., Schumann, A., Benninger, F., Feucht, M., Baer, K.J., Schlattmann, P., 2019. Brain-heart interactions considering complex physiological data: processing schemes for time-variant, frequency-dependent, topographical and statistical examination of directed interactions by convergent cross mapping. Physiol. Meas. 40, 114001. doi:10.1088/1361-6579/ab5050.

Schwabe, L., Haddad, L., Schachinger, H., 2008. HPA axis activation by a socially evaluated cold-pressor test. Psychoneuroendocrinology 33, 890–895. doi:10.1016/j.psyneuen.2008.03.001.

Sel, A., Azevedo, R.T., Tsakiris, M., 2017. Heartfelt self: cardio-visual integration affects self-face recognition and interoceptive cortical processing. Cereb. Cortex 27, 5144–5155. doi:10.1093/cercor/bhw296.

Shao, S., Shen, K., Wilder-Smith, E.P.V., Li, X., 2011. Effect of pain perception on the heartbeat evoked potential. Clin. Neurophysiol. 122, 1838–1845. doi:10.1016/j.clinph.2011.02.014.

Shao, S., Shen, K., Yu, K., Wilder-Smith, E.P.V., Li, X., 2012. Frequency-domain EEG source analysis for acute tonic cold pain perception. Clin. Neurophysiol. 123, 2042–2049. doi:10.1016/j.clinph.2012.02.084.

Silvani, A., Calandra-Buonaura, G., Dampney, R.A.L., Cortelli, P., 2016. Brain-heart interactions: physiology and clinical implications. Philos. Trans. A Math. Phys. Eng. Sci. 374. doi:10.1098/rsta.2015.0181.

Sterling, P., 2012. Allostasis: a model of predictive regulation. Physiol Behav. 106, 5–15. doi:10.1016/j.physbeh.2011.06.004, Allostasis and Allostatic Load.

Tahsili-Fahadan, P., Geocadin, R.G., 2017. Heart-brain axis: effects of neurologic injury on cardiovascular function. Circ. Res. 120, 559–572. doi:10.1161/CIRCRESAHA.116.308446.

Terhaar, J., Viola, F.C., Bär, K.J., Debener, S., 2012. Heartbeat evoked potentials mirror altered body perception in depressed patients. Clin. Neurophysiol. 123, 1950–1957. doi:10.1016/j.clinph.2012.02.086.

Thayer, J.F., Ahs, F., Fredrikson, M., Sollers, J.J., Wager, T.D., 2012. A meta-analysis of heart rate variability and neuroimaging studies: implications for heart rate vari-

ability as a marker of stress and health. Neurosci. Biobehav. Rev. 36, 747–756. doi:10.1016/j.neubiorev.2011.11.009.

Thayer, J.F., Lane, R.D., 2009. Claude Bernard and the heart–brain connection: further elaboration of a model of neurovisceral integration. Neurosci. Biobehav. Rev. 33, 81–88. doi:10.1016/j.neubiorev.2008.08.004, The Inevitable Link between Heart and Behavior: New Insights from Biomedical Research and Implications for Clinical Practice.

Valenza, G., Citi, L., Saul, J.P., Barbieri, R., 2018a. Measures of sympathetic and parasympathetic autonomic outflow from heartbeat dynamics. J. Appl. Physiol. 125, 19–39. doi:10.1152/japplphysiol.00842.2017.

Valenza, G., Citi, L., Wyller, V.B., Barbieri, R., 2018b. ECG-derived sympathetic and parasympathetic activity in the healthy: an early lower-body negative pressure study using adaptive Kalman prediction. In: Proceedings of the 40th Annual International Conference of the IEEE Engineering in Medicine and Biology Society (EMBC), pp. 5628–5631. doi:10.1109/EMBC.2018.8513512 Presented at the 2018 40th Annual International Conference of the IEEE Engineering in Medicine and Biology Society (EMBC).

Valenza, G., Greco, A., Gentili, C., Lanata, A., Sebastiani, L., Menicucci, D., Gemignani, A., Scilingo, E.P., 2016. Combining electroencephalographic activity and instantaneous heart rate for assessing brain–heart dynamics during visual emotional elicitation in healthy subjects. Philos. Trans. R. Soc. A 374, 20150176. doi:10.1098/rsta.2015.0176.

Valenza, G., Passamonti, L., Duggento, A., Toschi, N., Barbieri, R., 2020. Uncovering complex central autonomic networks at rest: a functional magnetic resonance imaging study on complex cardiovascular oscillations. J. R. Soc. Interface 17, 20190878. doi:10.1098/rsif.2019.0878.

Valenza, G., Sclocco, R., Duggento, A., Passamonti, L., Napadow, V., Barbieri, R., Toschi, N., 2019. The central autonomic network at rest: uncovering functional MRI correlates of time-varying autonomic outflow. Neuroimage 197, 383–390. doi:10.1016/j.neuroimage.2019.04.075.

Victor, R.G., Leimbach, W.N., Seals, D.R., Wallin, B.G., Mark, A.L., 1987. Effects of the cold pressor test on muscle sympathetic nerve activity in humans. Hypertension 9, 429–436. doi:10.1161/01.HYP.9.5.429.

Wang, L., Xiao, Y., Urman, R.D., Lin, Y., 2020. Cold pressor pain assessment based on EEG power spectrum. SN Appl. Sci. 2, 1976. doi:10.1007/s42452-020-03822-8.

Wang, X., Inui, K., Qiu, Y., Kakigi, R., 2004. Cortical responses to noxious stimuli during sleep. Neuroscience 128, 177–186. doi:10.1016/j.neuroscience.2004.06.036.

Weber, I., Niehaus, H., Krause, K., Molitor, L., Peper, M., Schmidt, L., Hakel, L., Timmermann, L., Menzler, K., Knake, S., Oehrn, C.R., 2021. Trust your gut: vagal nerve stimulation in humans improves reinforcement learning. Brain Commun. 3. doi:10.1093/braincomms/fcab039.